Journal of Applied Physics

Electron-spin-resonance and electrically detected-magnetic-resonance characterization on P_{bC} center in various 4H-SiC(0001)/SiO_2 interfaces

Cite as: J. Appl. Phys. **127**, 145301 (2020); https://doi.org/10.1063/1.5134648
Submitted: 01 November 2019 . Accepted: 18 March 2020 . Published Online: 09 April 2020

T. Umeda, Y. Nakano, E. Higa, T. Okuda, T. Kimoto, T. Hosoi, H. Watanabe, M. Sometani, and S. Harada

Journal of Applied Physics ARTICLE scitation.org/journal/jap

Electron-spin-resonance and electrically detected-magnetic-resonance characterization on P_{bC} center in various 4H-SiC(0001)/SiO_2 interfaces

Cite as: J. Appl. Phys. **127**, 145301 (2020); doi: 10.1063/1.5134648
Submitted: 1 November 2019 · Accepted: 18 March 2020 ·
Published Online: 9 April 2020

T. Umeda,[1,a)] Y. Nakano,[1] E. Higa,[1] T. Okuda,[2] T. Kimoto,[2] T. Hosoi,[3] H. Watanabe,[3] M. Sometani,[4] and S. Harada[4]

AFFILIATIONS

[1]Institute of Applied Physics, University of Tsukuba, Tsukuba 305-8573, Japan
[2]Graduate School of Engineering, Kyoto University, Kyoto 615-8510, Japan
[3]Graduate School of Engineering, Osaka University, Osaka 565-0871, Japan
[4]National Institute of Advanced Industrial Science and Technology (AIST), Tsukuba 305-8569, Japan

Note: This paper is part of the Special Topic on Defects in Semiconductors 2020.
[a)]**Author to whom correspondence should be addressed:** umeda@bk.tsukuba.ac.jp

ABSTRACT

We characterized an intrinsic interface defect, called the "P_{bC} center," formed at 4H-SiC(0001)/SiO_2 interfaces by means of electron-spin-resonance (ESR) and electrically detected-magnetic-resonance (EDMR) spectroscopies. The formation of the P_{bC} center was observed with a spin density of $3–4 \times 10^{12}$ cm^{-2} after standard thermal oxidation. This center could be effectively removed by the NO post-oxidation-anneal (POA) process or ultra-high-temperature oxidation and could be passivated by H atoms via the H_2 POA process. There was a clear correlation between the P_{bC} center and field-effect mobility (μ_{FE}) of 4H-SiC(0001) metal–oxide–semiconductor field effect transistors (MOSFETs). The P_{bC} center decreased μ_{FE} because this center acts as electron traps, reducing the free-carrier density in the inversion channel of 4H-SiC (0001) MOSFET. We also examined the counter doping effect of NO POA by introducing ^{15}N impurities; however, the counter doping of ^{15}N donors was not detectable by ESR (much lower than 2×10^{11} cm^{-2}). Highly sensitive EDMR measurements revealed that the P_{bC} center has two isotropic hyperfine (HF) interactions at 1.3 and 6.8 mT and suggested that its main ^{13}C HF interaction should be larger than 14 mT. Based on the present experimental data, the origin of the P_{bC} center was ascribed as a carbon-related interface defect that forms a C–H bond after hydrogen passivation. This feature is similar to that of the *porous*-P_{bC} centers (carbon dangling-bond centers) found in *porous*-SiC/SiO_2 systems. However, their HF signatures indicated that the P_{bC} center at 4H-SiC(0001)/SiO_2 interfaces and the *porous*-P_{bC} centers in *porous*-SiC should be different centers associated with different wave functions.

I. INTRODUCTION

The 4H-SiC/SiO_2 interface is the key part for 4H-SiC metal–oxide–semiconductor field effect transistors (MOSFETs) and is a benchmark system for every wide-bandgap semiconductor MOS interface.[1] The standard method for fabricating good 4H-SiC/SiO_2 interfaces is thermal oxidation by dry O_2 gas (dry oxidation) followed by interfacial nitridation such as NO post-oxidation anneal (POA).[2] This process can reduce shallow interface states near the conduction band edge (E_C)[2,3] and deeper electron traps,[4] resulting in a drastic improvement on the field-effect mobility (μ_{FE}) of SiC-MOSFETs. As a result, the improved μ_{FE} reaches 30–40 $cm^2 V^{-1} s^{-1}$ for 4H-SiC(0001) (so-called "Si face") MOS interfaces, realizing ultra-low-energy-loss performances of power SiC-MOSFETs as compared to those of conventional power Si-MOSFETs.[1,5] However, the improved μ_{FE} is still orders of magnitude lower than the electron mobility of 1000 $cm^2 V^{-1} s^{-1}$ in bulk 4H-SiC. Therefore, many challenges have been made for further improving μ_{FE}, such as phosphorous (P) incorporation by $POCl_3$ POA,[6] boron incorporation,[7] Ba incorporation,[8] hydrogen (H) incorporation by "wet-POA,"[9] counter doping of shallow donors

into the channel region,[10] and oxidation techniques without any additive elements.[11]

Recently, we reported an electron-spin-resonance (ESR) observation on carbon-related paramagnetic defects at the 4H-SiC(0001)/SiO_2 interface,[12] which correlate closely to the improvements on μ_{FE}. They were intrinsically formed by the dry oxidation of 4H-SiC(0001) surfaces and were successfully removed by NO POA or $POCl_3$ POA. Their typical density was $3–4 \times 10^{12}\,cm^{-2}$, which is high enough for affecting μ_{FE} drastically. We found that their ESR signal has some similarities to previous ESR signals called "P_{bC} centers."[13,14] The P_{bC} centers were originally found in *porous*-SiC/SiO_2 interfaces and have been identified as carbon dangling-bond (DB) centers with several different orientations.[13] The name of "P_{bC}" comes from its analogy to the P_b centers (Si DB centers[15]) at Si/SiO_2 interfaces. Here, we distinguish our P_{bC} center in 4H-SiC(0001) and the P_{bC} centers in *porous*-SiC; we call the former one as "P_{bC} center" and the latter one as "*porous*-P_{bC} centers." The reason for this distinction originates from spectroscopic differences between two types of P_{bC} centers, which will be described later.

In this paper, we characterize the P_{bC} center at 4H-SiC(0001)/SiO_2 interfaces in more detail by employing two techniques: one is conventional ESR spectroscopy[12] and another is electrically detected-magnetic-resonance (EDMR) spectroscopy[16–19] enabling electrical detection of ESR signals. ESR can give us spin densities of the P_{bC} center. Using this technique, we examined a correlation between the P_{bC} center and μ_{FE} for a wide variety of 4H-SiC(0001)/SiO_2 interfaces prepared by a ultra-high-temperature (UHT) oxidation process[11] and an ^{15}NO POA process. The former process can achieve several times higher μ_{FE} without adding any intentional impurities. The latter process enables us to monitor ^{15}N impurities introduced by the counter doping mechanism.[10] Furthermore, we demonstrate that the P_{bC} center can be passivated via the H_2 POA process, likewise the *porous*-P_{bC} centers[14] and the original P_b centers.[15] In the next place, we discussed the origin of the P_{bC} center on the basis of EDMR data. EDMR achieved an excellent sensitivity to the P_{bC} center in real 4H-SiC(0001) MOSFETs. Taking advantage of higher sensitivity, we focused on spectroscopic features of the P_{bC} center, in particular, hyperfine (HF) interactions between its electron spin and surrounding nuclear spins.

II. EXPERIMENTAL

The P_{bC} center was detected by both ESR and EDMR spectrometers. For ESR measurements, we used a Bruker E500 continuous-wave X-band spectrometer equipped with a super-high-Q cavity and an Oxford ESR900 continuous-flow liquid He cryostat. All spectra were measured using magnetic-field modulation at 100 kHz and microwave excitation at 9.43 GHz. The P_{bC} center was observed at room temperature because room-temperature ESR spectra simply consisted of the P_{bC} signal and an E' signal from a SiO_2 sample rod. On the other hand, the shallow N donors were measured at either 20 K or 50 K. The photo-excitation (100-W Halogen light) was used in low-temperature measurements because the shallow donors were partially compensated in our substrates. Magnetic field (**B**) was usually set to a surface-normal direction (**B** parallels to the *c* axis or the [0001] axis) unless otherwise stated. Magnetic-field values were calibrated by a built-in nuclear-magnetic-resonance (NMR) tesla meter with an accuracy of 0.01 mT or finer.

Since ESR measures the whole of the substrate, we have to carefully prepare ultra-high-quality 4H-SiC(0001) substrates to observe interface defects. We used full-epitaxial-layer substrates with very low N or Al concentrations ($4 \times 10^{14}\,cm^{-3}$). Both front and back surfaces of the substrate were finished by the chemical mechanical polish (CMP) process. For most of the substrates, we have further carried out surface cleaning by dry etching, which we call a "reset process."[12] The effect of the reset process can be seen in Sec. III A. Using 4H-SiC(0001) faces of such substrates, we characterized an UHT oxidation process and a ^{15}NO POA process. Table I describes details of the ESR samples and processes. The UHT oxidation samples were prepared by the same UHT furnace and the same experimental procedure as used in previous works.[11] For the ^{15}NO POA experiment, we prepared a ^{15}NO gas with ^{15}N

TABLE I. List of 4H-SiC(0001) ESR samples. All substrates are 4H-SiC(0001) full-epitaxial layers with both-side CMP finishing. Oxidations and POA processes were done at atmospheric pressure. Just before oxidation, standard RCA surface cleaning was subjected to substrates. After oxidation, the back-side SiO_2 layer (i.e., a C-face oxide layer) was removed by one-side HF etching.[12] Field-effect mobilities (μ_{FE}) shown here are maximum values.

4H-SiC(0001) ESR samples	Process	SiO_2 thickness (nm)	P_{bC} density ($\times 10^{12}\,cm^{-2}$)	μ_{FE} ($cm^2\,V^{-1}\,s^{-1}$)
Dry (Ref)[a]	Dry oxidation at 1200 °C by 100% O_2	30	3.2	3.0[d]
Dry (UHT ox.)[a]	Dry oxidation at 1600 °C by 0.3% O_2 + 97.7% Ar	30	0.7	9.7[d]
Substrate[b]	Only the same surface cleaning process	0	…	…
Dry (Normal)[b]	Dry oxidation at 1200 °C by 100% O_2	50	3.8	7.2[e]
Dry (Normal) + ^{15}NO[b]	"Dry (Normal)" after ^{15}NO POA (1.1% ^{15}NO + 98.9% N_2) at 1440 °C for 20 min	50	0.5	20.5[e]
Dry (Normal) + NO[c]	"Dry (Normal)" after NO POA at 1250 °C for 60 min	50	<0.1[12]	32[e]

[a]Epitaxial layer with [N] = $4 \times 10^{14}\,cm^{-3}$ and 100 μm-thick, subjected to the reset process + RCA cleaning before oxidation.
[b]Epitaxial layer with [N] = $4 \times 10^{14}\,cm^{-3}$ and 160 μm-thick, subjected to sacrificed oxidation cleaning + RCA cleaning before oxidation.
[c]Epitaxial layer with [Al] = $4 \times 10^{14}\,cm^{-3}$ and 130 μm-thick, subjected to the reset process + RCA cleaning before oxidation.[12]
[d]MOSFETs were fabricated on 4°-off *p*-type epitaxial layer ([Al] = $5 \times 10^{15}\,cm^{-3}$).[11]
[e]MOSFETs were fabricated on 4°-off *p*-type epitaxial layer ([Al] = $1 \times 10^{15}\,cm^{-3}$).

enrichment = 100%. The POA temperature was set to be higher than the standard condition (1250 °C[4,12] → 1440 °C) because we aimed for interfacial nitridation as complete as possible using a diluted ^{15}NO atmospheric mixture (1.1% ^{15}NO + 98.9% Ar). Together with ESR samples, lateral *n*-channel 4H-SiC(0001) MOSFET samples were also prepared for electrical characterizations. Maximum μ_{FE} values are listed in the table.

For H_2 POA experiments, we used 100% H_2 gas and the same experimental setup used in our previous studies.[20,21] Using this setup, we successfully observed the H-passivation behaviors of lifetime-killer centers in *p*-type epitaxial layers[20] and even those of intrinsic defects in thick substrates.[21] We also carried out a H-dissociation experiment by Ar-gas annealing at 900 °C.

For EDMR measurements, we prepared lateral *n*-channel 4H-SiC(0001) MOSFETs on an optimum 4°-off p^--type epitaxial layer ($[Al] = 1 \times 10^{15}\,cm^{-3}$). A gate SiO_2 layer (30 nm) was formed by standard dry oxidation as used for the ESR samples. The MOSFETs with an optimum gate size (gate length/width = 5/2000 μm) were characterized by a home-built EDMR spectrometer based on a Bruker ESP300 X-band spectrometer. The magnetic-field modulation frequency was set to 1.5 kHz for an optimum signal-to-noise ratio (*S*/*N*). To enhance EDMR signals of the P_{bC} center, we adopted the bipolar-amplification-effect (BAE) EDMR technique developed by Aichinger and Lenahan.[17] In this regime, we activated a constant drain current of −10 μA (a negative sign means a forward-biased current) and monitored a source current by an EDMR (spin-dependent current) detector. Then, by varying a gate bias, we searched for the best BAE EDMR signals arising from paramagnetic interface states. The highest *S*/*N* figure was obtained for a source current of ∼200 nA and a gate bias of approximately −8 V in our MOSFETs. All EDMR measurements were carried out at room temperature and microwave excitation at 9.46 GHz and 200 mW. For EDMR, magnetic-field values were calibrated by an Echo Electronics EFM-2000 NMR tesla meter with an accuracy of the order of 0.01 mT.

III. ESR RESULTS

A. Formation of the P_{bC} center

Here we examine the formation behavior of the P_{bC} center, which is the following work of our previous paper.[12] Figures 1 and 2 show ESR studies on two different types of substrates (see Table I). The substrates examined in Fig. 1 were prepared without the reset process.[12] An isotropic broad ESR signal appeared at the *g* factor (*g*) of 2.003, which is most probably due to residual carbons on the surface.[12] This signal could not be eliminated even by sacrificed oxidation cleaning (surface oxidation + HF etching). However, after standard dry oxidation (50-nm growth), we can observe an appreciable increase in the ESR signal, which is due to the formation of the P_{bC} center. By extracting the increment of the signal, the spin density of the P_{bC} center was estimated to be $3.8 \times 10^{12}\,cm^{-2}$.

On the other hand, a series of ESR spectra shown in Fig. 2 were obtained by taking advantage of the reset process. As shown in (a), the residual-carbon ESR signal completely disappeared after the reset process, showing a flat baseline except the *E*′ signal. After dry oxidation (30-nm growth), the P_{bC} center with $3.2 \times 10^{12}\,cm^{-2}$ was clearly detected as shown in (b). We always found spin

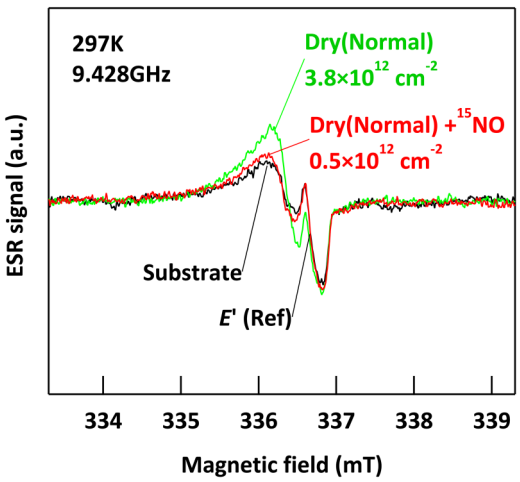

FIG. 1. ESR measurements on the P_{bC} center at the 4H-SiC(0001)/SiO_2 interface and after the ^{15}NO POA process (see the sample list in Table I). ESR spectra were measured under a microwave excitation of 0.2 mW and a modulation amplitude of 0.25 mT.

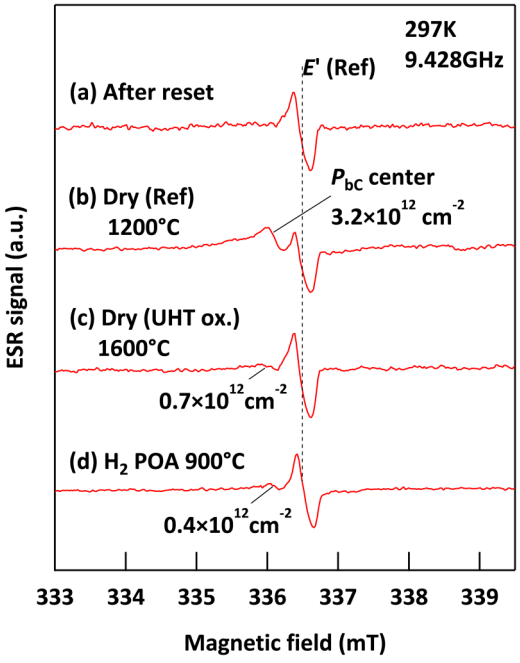

FIG. 2. ESR spectra of the P_{bC} center in various 4H-SiC(0001)/SiO_2 interfaces (see the sample list in Table I). (a) After the reset process (surface dry etching). (b) After standard dry oxidation at 1200 °C. (c) After ultra-high-temperature (UHT) oxidation at 1600 °C. (d) After H_2 POA at 900 °C. All ESR spectra were measured after C-face-oxide etching, and ESR signals arise from the Si-face side, except a reference *E*′ signal from a sample rod. All ESR spectra were measured under a microwave excitation of 0.2 mW and a modulation amplitude of 0.25 mT.

densities of P_{bC} in the range between 3×10^{12} and $4 \times 10^{12}\,cm^{-2}$, independent of oxide thicknesses from 10 to 60 nm.

It is worth noting that the above spin densities measured for the n^--type substrates were nearly equal to those measured for the p^--type substrates.[12] This suggests that the surface Fermi level approached the same position in both types of substrates. Possibly the P_{bC} center may pin the surface Fermi level close to its energy level. Since the P_{bC} center is considered as a spin-1/2 paramagnetic center (judging from the absence of any fine splittings), its one-electron energy level can capture an additional electron. Namely, each P_{bC} center acts as an electron trap. When the inversion channel is going to form in an n-channel 4H-SiC(0001) MOSFET, the P_{bC} center captures free electrons at the outset. After filling out all the energy levels of the P_{bC} center, the Fermi level can be released from there, moving toward E_C for a strong inversion condition. This is a mechanism of how the P_{bC} center affects electrical characteristics of the 4H-SiC(0001) MOSFET.

B. Removing the P_{bC} center by UHT oxidation and POA processes

Previously, we reported that the P_{bC} center can be eliminated by optimum NO POA and $POCl_3$ POA.[12] We here confirm whether the P_{bC} center can also be removed by controlling oxidation conditions alone and without any additive impurities. Figure 2(c) shows an ESR spectrum measured after an optimum UHT oxidation at 1600 °C (see Table I), which clearly indicates a successful reduction in the P_{bC} signal. The P_{bC} density decreased to $0.7 \times 10^{12}\,cm^{-2}$. The UHT oxidation used here was developed to maximize the removal of residual-carbon atoms by tuning both oxygen partial pressure and oxidation temperature toward a passive oxidation–active oxidation boundary.[11] The ESR result demonstrates the removal of carbon-related defects (the P_{bC} centers), supporting the above concept from a microscopic viewpoint.

In Fig. 1, we examine the ^{15}NO POA effect on the P_{bC} center. After the ^{15}NO POA process, the ESR signal almost returned to the original signal (before oxidation), indicating the annihilation of the P_{bC} center. The remaining density of P_{bC} was estimated to be $0.5 \times 10^{12}\,cm^{-2}$. This value is larger than that of an optimum NO POA process ($\leq 0.1 \times 10^{12}\,cm^{-2}$),[12] implying some incompleteness of the interfacial nitridation.

C. Influence of the P_{bC} center on μ_{FE}

Figure 3 summarizes a relationship between the P_{bC} signals and the maximum μ_{FE} values. Basically, removing the P_{bC} center increased the top values of μ_{FE}. This behavior is reasonable because as we mentioned in Sec. III A, the P_{bC} center has a role of reducing the free-carrier density in the inversion channel of the 4H-SiC (0001) MOSFET. Note that μ_{FE} depends on both the mobility and the density of the free carriers.[4] The removal of the P_{bC} centers directly connects to a higher free-carrier density, resulting in a higher μ_{FE}. Since the P_{bC} density of $3–4 \times 10^{12}\,cm^{-2}$ is just comparable with the free-carrier density in the inversion channel,[3,4] the P_{bC} center strongly suppresses μ_{FE}. In Sec. III E, we will demonstrate using ^{15}N impurities that the counter doping effect due to NO POA was much weaker than the effect of removing the P_{bC} centers. Therefore, the improved μ_{FE} shown in Fig. 3 originates

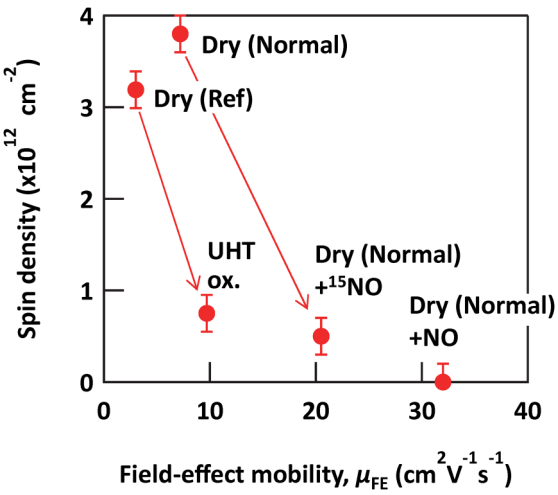

FIG. 3. Spin densities of the P_{bC} center versus maximum μ_{FE} values.

primarily from the removal of the P_{bC} centers. In addition, the reduction in the shallow interface states, which were clearly detected in the range between $E_C - 0$ eV and $E_C - 0.7$ eV after NO POAs,[3,4] will also contribute to the improvement.

D. Hydrogen passivation of the P_{bC} center

Another way for reducing the influence of the P_{bC} center may be H passivation. Such passivation is well established for the original P_b centers at Si/SiO_2 interfaces.[15] Moreover, in *porous*-SiC/SiO_2, H passivation of the *porous*-P_{bC} centers was observed by a forming-gas POA (H_2 5% + N_2 95%) at 400 °C, resulting in a drastic reduction in the *porous*-P_{bC} signal (<5% of the original intensity before the POA).[14] We, therefore, examined H passivation of the P_{bC} center in 4H-SiC(0001) using the H_2 POA process.

Figure 4 shows normalized intensities of the P_{bC} signal, which represent the passivation rate (%) as a function of H_2 POA temperature. Efficient passivation was observable only at around 900 °C. The largest passivation rate was 10%–40% depending on the H_2 POA time. It seems that H passivation of the P_{bC} center is not as easy as the cases of the P_b center (efficient passivation was available at 220–550 °C[15]) and the *porous*-P_{bC} centers (H passivation started at 400 °C and maintained up to 800 °C[14]). This result may be in line with our common knowledge that 4H-SiC(0001)/SiO_2 interfaces are generally insensitive to the incorporation of H atoms so that other additive impurities (N, B, P, Ba, etc.) have been tried so far.[1] Nevertheless, the present result shows the potential ability of H passivation if the passivation condition is carefully designed. Actually, the "wet-POA process" (the POA process by H_2O ambient)[9] was proposed for obtaining good 4H-SiC(0001)/SiO_2 interfaces comparable to those after NO POA. We speculate that such a process may realize an efficient H passivation of the P_{bC} center.

As seen in Fig. 4, Ar annealing at 900 °C or H_2 POA over 900 °C caused the recovery of the P_{bC} signal due to dissociation of

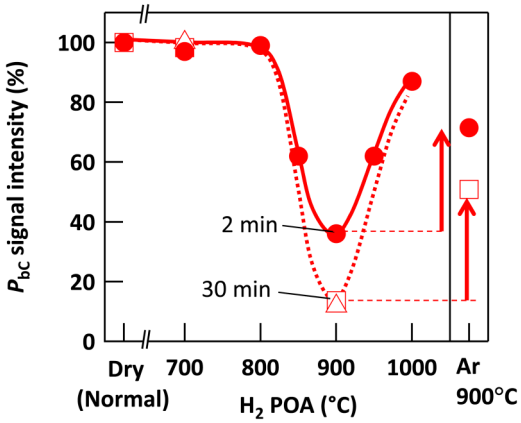

FIG. 4. H passivation of the P_{bC} center by the H_2 POA process. Solid circles were measured for H_2 POA for 2 min on 4H-SiC(0001)/SiO_2 (50-nm thick). Open squares and open triangles were taken for H_2 POA for 30 min on 4H-SiC (0001)/SiO_2 with 44 nm and 10 nm in oxide thicknesses, respectively. Solid and dashed curves are guides for eyes. Right-hand-side symbols show H-dissociation experiments by Ar anneal for 30 min.

H atoms. Note that this temperature range is consistent with the dissociation temperature of C–H bonds.[14,21] The *porous*-P_{bC} centers exhibited the same dissociation behavior above 850 °C.[14] Accordingly, it is reasonable to consider that the P_{bC} center forms a C–H bond when H passivation combines a H atom with its unpaired electron.

E. ^{15}N doping by the ^{15}NO POA process

In the present NO POA experiment using ^{15}NO, we can distinguish residual ^{14}N donors in the substrate and interfacial ^{15}N donors intentionally doped by NO POA. As tabulated in Table II, ^{14}N and ^{15}N isotopes have different nuclear spins ($I = 1$ and 1/2, respectively), which generate a triplet HF splitting for ^{14}N or a doublet HF splitting for ^{15}N. Since the HF interactions of shallow ^{14}N donors in 4H-SiC are already well known (see Table II),[24] we can accurately predict those of shallow ^{15}N donors via the following procedure. From the known ^{14}N HF tensor ($A_{//}$ and $A_{\perp}$ principal values), the isotropic and anisotropic HF parameters (A_{iso} and A_{aniso}, respectively) are derived using the equations $A_{iso} = (A_{//} + 2A_{\perp})/3$ and $A_{aniso} = (A_{//} - A_{\perp})/3$.[22,23] Ratios of A_{iso}/A_0 and A_{aniso}/b_0 represent 2*s*- and 2*p*-orbital fractions on a ^{14}N donor, where A_0 and b_0 are HF constants for pure 2*s*- and 2*p*-orbitals of ^{14}N.[22] Supposing the same 2*s*- and 2*p*-orbital fractions on a ^{15}N donor (it is a quite reasonable assumption), we then obtain the A_{iso} and A_{aniso} values for a ^{15}N donor and subsequently its $A_{//}$ and $A_{\perp}$ values, too. The predicted ^{15}N HF splitting is 2.55 mT for the ^{15}N (*k*) donor and is 0.15 mT for the ^{15}N(*h*) donor, when **B** // [0001].

In Fig. 5, we independently examine ^{15}N(*k*) and ^{15}N(*h*) donor signals by comparing the ^{15}NO POA samples before and after the POA. In every ESR spectrum, the ^{14}N donor signals were dominant, which arise from residual donors in the n^--type substrates. For the ^{15}N(*k*) donor, its doublet signal must appear as simulated in Fig. 5(a). However, we hardly detected such a doublet signal in the experimental spectrum, and the ESR spectra before and after ^{15}NO POA involved only the ^{14}N(*k*) donor signal with a spin density of 1.8×10^{12} cm^{-2} or 1.1×10^{14} cm^{-3}. The ^{15}N(*k*) density must be smaller than 1×10^{11} cm^{-2}. The situation seems to be similar for the ^{15}N(*h*) donor [Fig. 5(b)]. Although small HF splittings of ^{14}N(*h*) and ^{15}N(*h*) do not allow to separate these two donor signals, the ESR spectra before and after ^{15}NO POA can be accounted for only the ^{14}N(*h*) donor signal. In fact, a spectral simulation [a dotted curve in Fig. 5(b)] calculating the ^{14}N(*h*) donor signal (a blue solid line, a spin density of 3.7×10^{12} cm^{-2}) + a carbon signal (a gray solid line) perfectly reproduced the experimental spectrum. We, therefore, judged that the contribution of the ^{15}N(*h*) donors must be smaller than 1×10^{11} cm^{-2} [see a simulated ^{15}N donor signal in Fig. 5(b)]. Accordingly, there was no detectable counter doping of ^{15}N in the ^{15}NO POA experiment. Totally, the counter doping density must be rather smaller than 2×10^{11} cm^{-2}. Note that the observed spin density of the ^{14}N donors [^{14}N(*k*) + ^{14}N(*h*)] is 3.4×10^{14} cm^{-3}, which is similar to the doping

TABLE II. HF constants (A_0 and b_0[22]) and HF parameters ($A_{//}$, $A_{\perp}$, A_{iso}, and A_{aniso}[22,23]) of shallow ^{14}N and ^{15}N donors. ^{14}N HF parameters are experimental values,[24] which are converted in mT via 1 mT = 28.02 MHz. ^{15}N HF parameters are predicted from ^{14}N experimental values (see details in the text). All HF tensors are *c*-axial symmetric; i.e., their $A_{//}$ principal values correspond to HF splittings when **B** // [0001].

Nuclear spin (I) (natural abundance)	HF constants[22]	HF parameters	
		k site, N(*k*)	*h* site, N(*h*)
^{14}N ($I = 1$) (99.63%)	$A_0 = 64.6$ mT $b_0 = 1.98$ mT	$A_{//} = 1.82$ mT $A_{\perp} = 1.82$ mT $A_{iso} = 1.82$ mT $A_{aniso} < 0.001$ mT	$A_{//} = 0.11$ mT $A_{\perp} = 0.10$ mT $A_{iso} = 0.10$ mT $A_{aniso} = 0.003$ mT
^{15}N ($I = 1/2$) (0.37%)	$A_0 = 90.6$ mT[a] $b_0 = 2.78$ mT[a]	$A_{//} = 2.55$ mT $A_{\perp} = 2.55$ mT $A_{iso} = 2.55$ mT[b] $A_{aniso} < 0.001$ mT[b]	$A_{//} = 0.15$ mT $A_{\perp} = 0.14$ mT $A_{iso} = 0.145$ mT[b] $A_{aniso} = 0.004$ mT[b]

[a]1.40 times of the HF constants of ^{14}N.[22]
[b]1.40 times of the measured HF parameters (A_{iso} and A_{aniso}) of ^{14}N.

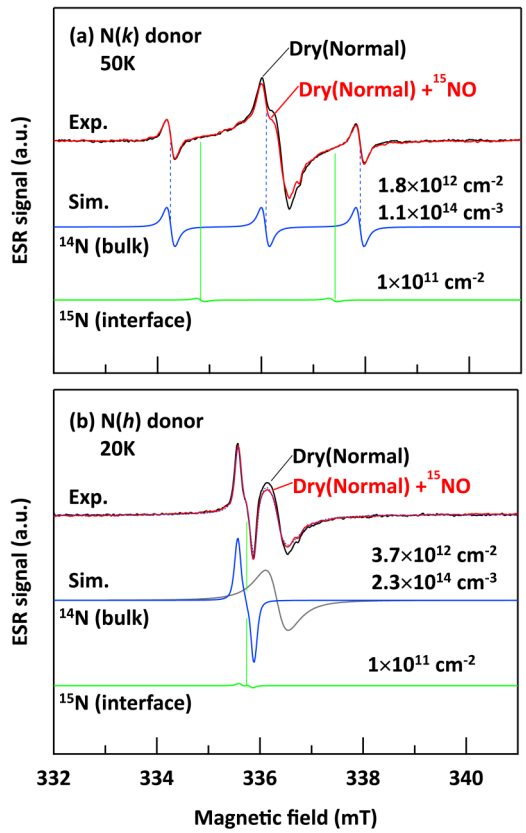

FIG. 5. ESR studies on ^{15}N doping after ^{15}NO POA on 4H-SiC(0001)/SiO_2. (a) N(k) donors measured at 50 K under photo-excitation and a microwave power of 0.2 mW. (b) N(h) donors measured at 20 K under photo-excitation and a microwave power of 0.02 mW. ^{14}N and ^{15}N donor signals were simulated by adopting HF parameters shown in Table II. The ^{15}N donor signal was simulated by assuming a spin density of 1×10^{11} cm^{-2}. The dotted curve in (b) is a simulated spectrum by calculating a combination of the ^{14}N donor signal (blue solid line) + carbon signal (gray solid line).

density of our epitaxial layer (4×10^{14} cm^{-3}). This consistency ensures the validity of the above ESR evaluation.

We finally mention that the above conclusion was also consistent with the previous result.[12] Using the p^--type substrate (Table I), the counter doping was also estimated to be $<1 \times 10^{11}$ cm^{-2} for an optimum NO POA condition[12] [the same as "Dry (Normal) + NO" shown in Fig. 3]. It is a striking contrast with the case of $POCl_3$ POA, which caused a strong counter doping of P donors over 1×10^{12} cm^{-2} (Ref. 12). We speculate that such a strong counter doping brings a maximum μ_{FE} of 100 cm^2 V^{-1} s^{-1} (Ref. 6).

IV. EDMR RESULTS

As was seen in the preceding section, the P_{bC} center is an important interface defect that is related closely to the improved μ_{FE}. The next major interest is its microscopic origin. To achieve a conclusive identification, we must analyze HF interactions of the

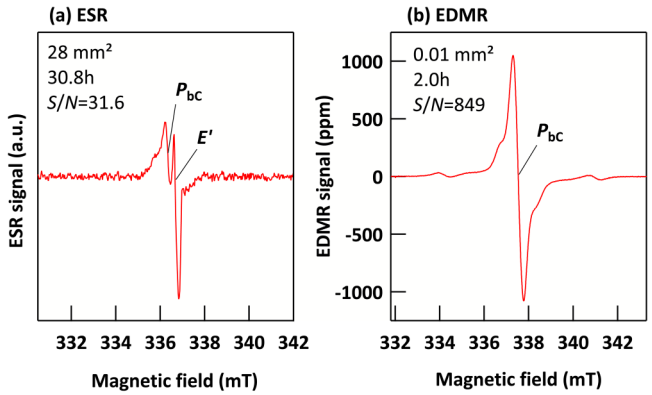

FIG. 6. Observation of the P_{bC} center by means of ESR and EDMR spectroscopy. (a) Typical ESR spectrum measured for a 28-mm^2 specimen prepared by a "Dry (Ref)" condition (using a microwave power of 0.2 mW and a modulation amplitude of 0.25 mT). An E' signal (a SiO_2 defect) arises from a sample quartz rod. (b) EDMR spectrum measured for 4H-SiC(0001) MOSFET with a 0.01-mm^2 gate area prepared by a "Dry (Ref)" condition (using a microwave power of 200 mW and a modulation amplitude of 0.5 mT). Signal-to-noise ratios (S/N) shown here are calculated as follows: (peak-to-peak height of P_{bC} signal)/(root-mean-square noise level).

P_{bC} center, especially, due to a nuclear spin of ^{13}C ($I = 1/2$, natural abundance = 1.1%). However, it was a very hard task for conventional ESR spectroscopy. A typical ESR signal of the P_{bC} center [Fig. 6(a)] shows only $S/N \sim 30$ for over 1-day accumulation. To observe a ^{13}C HF satellite signal (relative intensity = 0.55% of the total signal) with $S/N = 10$, we will need 4240-day accumulation. Moreover, its ESR signal suffered from a strong microwave saturation behavior at low temperatures because the P_{bC} center is a carbon-related defect that involves only a weak spin-lattice relaxation as compared to any Si-related defects. This feature prevents us from a low-temperature signal enhancement on the P_{bC} center.

Therefore, we alternatively employed EDMR spectroscopy for this purpose. By optimizing EDMR measurements on our 4H-SiC (0001) MOSFETs (noted in Sec. II), a very strong EDMR signal of the P_{bC} center was observable, as shown in Fig. 6(b). The S/N figure reached 850 for only 2-hours accumulation. Accordingly, the EDMR spectrum clearly exhibits the presence of HF satellite signals. In principle, only 0.4-day accumulation is enough for resolving a ^{13}C HF satellite signal with $S/N = 10$ using EDMR.

Figure 7(a) focuses on weak HF satellite signals of the P_{bC} center. Within a 14-mT range examined here, all EDMR lines were nearly isotropic, which are also plotted in Fig. 7(b). We could not detect the known ^{13}C HF splitting of the *porous*-P_{bC} centers [$A_{iso} = 5.1$ mT (48×10^{-4} cm^{-1}) and $A_{aniso} = 1.4$ mT (13×10^{-4} cm^{-1})].[13] It is thus clear that the P_{bC} center in 4H-SiC (0001) is different from the *porous*-P_{bC} centers in *porous*-SiC. For the P_{bC} center, we found two isotropic HF splittings of 1.3 and 6.8 mT, as shown in Fig. 7(b). These HF splittings are also clearly different from those of an "interfacial Si-vacancy center" (^{13}C HF splittings = 1.3 mT and 2.8 mT when **B** // [0001]) observed in 4H-SiC(0001) MOSFETs.[25]

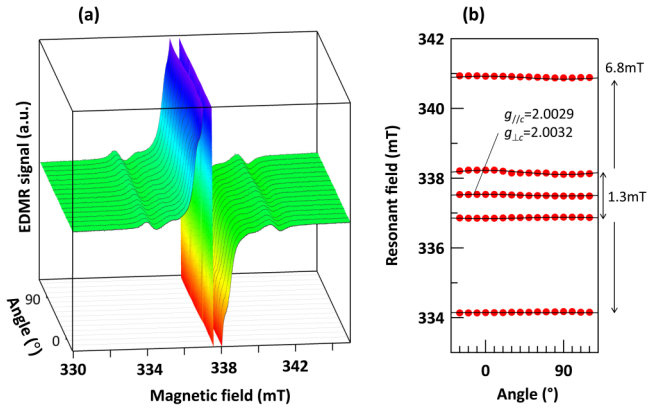

FIG. 7. (a) Magnified EDMR spectra as a function of a magnetic-field angle. Angles of 0° and 90° correspond to **B** parallel to [0001] and [11$\bar{2}$0], respectively. The modulation amplitude was set to be 0.5 mT for focusing on weak HF satellite signals. (b) Angular map of a P_{bC} EDMR signal. Solid lines are simulated results.

The largest HF interaction observed at 6.8 mT corresponds to only 5% of the isotropic HF constant of ^{13}C (134.77 mT[22]) or 4% of that of ^{29}Si (163.93 mT[22]). Namely, it originates from a minor part of the wave function of the P_{bC} center; in other words, the main HF interaction should appear outside the 14-mT range. Actually, we recently found the A_{iso} value of 18.9 mT for a ^{13}C HF interaction of the P_{bC}.[26] This large A_{iso} value means a strong *s*-character for the wave function of the P_{bC} center. Detailed analyses of its ^{13}C and ^{29}Si HF interactions are described in a recent paper.[26] The reason for the strong *s*-character can be accounted for using a carbon-adatom DB model based on first-principles calculations.[26]

We mention that the strong *s*-character of the P_{bC} center is consistent with its nearly isotropic *g* factor. An angular-dependence simulation shown in Fig. 7(b) (solid lines) nominally finds $g_{//c} = 2.0029$ and $g_{\perp c} = 2.0032$ for the P_{bC} center. This nearly isotropic *g* factor is reasonable because an anisotropic *g* factor is caused by the *p*-character of an unpaired electron.[15,22,23] The *g* factors estimated from EDMR seem to be deviated from those observed by ESR ($g_{//} = 2.0023$ and $g_{\perp} = 2.0032$[12]). Since an accurate determination of the *g* factors was difficult for the P_{bC} center because of its relatively large signal width, we judged that EDMR and ESR observed the same P_{bC} signal. At least, the observed *g* factors are close to the free-electron *g* factor (2.0023), supporting that the P_{bC} center is a carbon-related defect. The atomic model of the P_{bC} center is given in Ref. 26.

V. SUMMARY

We have studied the P_{bC} center intrinsically formed at 4H-SiC (0001)/SiO_2 interfaces. This center is a dominant carbon-related interface defect and played an important role in changing μ_{FE}. The present study demonstrated that the P_{bC} center can be removed by the NO POA process[2–4,12] and the UHT oxidation process,[11] resulting in lower P_{bC} densities and simultaneously higher μ_{FE}. This correlation was ascribable to that the P_{bC} center acts as electron traps, reducing the free-carrier density in the inversion channel of 4H-SiC(0001) MOSFET. We also demonstrated another way for deactivating the P_{bC} center using the H_2 POA process at 900 °C. This is so-called the H passivation effect, similar to the cases of the P_b centers in Si/SiO_2 systems and the *porous*-P_{bC} centers in *porous*-SiC. The H passivation suggests the formation of a C–H bond, supporting a recent C DB model for the P_{bC} center.[26] On the other hand, we could not detect the counter doping of shallow ^{15}N donors in the ^{15}NO POA experiment; the doping density should be much below 2×10^{11} cm^{-2}, which is smaller than 1/10 of the P_{bC} density ($3–4 \times 10^{12}$ cm^{-2}). The P_{bC} center was also detectable with an extremely high-*S*/*N* using EDMR spectroscopy on 4H-SiC(0001) MOSFETs. According to the high-*S*/*N* EDMR data, (1) the P_{bC} center has two sets of nearly isotropic HF interactions at 6.8 mT and 1.3 mT, (2) its main ^{13}C HF interaction is larger than 14 mT, and (3) the P_{bC} center is different from the *porous*-P_{bC} centers in *porous*-SiC[13,14] as well as the Si-vacancy center in 4H-SiC MOSFETs.[16,17,25]

ACKNOWLEDGMENTS

This work was supported by the Council for Science, Technology and Innovation (CSTI), Cross-ministerial Strategic Innovation Promotion Program (SIP), and "Next-generation power electronics" (funding agency: NEDO). This work was also partly supported by a Grant-in-Aid (Grant No. 17H02781) from the Ministry of Education, Culture, Sports, Science and Technology of Japan.

REFERENCES

[1]G. Liu, B. R. Tuttle, and S. Dhar, Appl. Phys. Rev. **2**, 021307 (2015).
[2]G. Y. Chung, C. C. Tin, J. R. Williams, K. McDonald, R. K. Chanana, R. A. Weller, M. Di Ventra, S. T. Pantelides, L. C. Feldman, O. W. Holland, M. K. Das, and J. W. Palmour, IEEE Electron Device Lett. **22**, 176 (2001).
[3]H. Yoshioka, J. Senzaki, A. Shimozato, Y. Tanaka, and H. Okumura, AIP Adv. **5**, 017109 (2015).
[4]T. Hatakeyama, Y. Kiuchi, M. Sometani, S. Harada, D. Okamoto, H. Yano, Y. Yonezawa, and H. Okumura, Appl. Phys. Express **10**, 046601 (2017).
[5]T. Kimoto and J. A. Cooper, *Fundamentals of Silicon Carbide Technology* (Wiley, Singapore, 2014).
[6]D. Okamoto, H. Yano, T. Hatayama, and T. Fuyuki, Appl. Phys. Lett. **96**, 203508 (2010).
[7]D. Okamoto, M. Sometani, S. Harada, R. Kosugi, Y. Yonezawa, and H. Yano, IEEE Electron Device Lett. **35**, 1176 (2014).
[8]D. J. Lichtenwalner, L. Cheng, S. Dhar, A. Agarwal, and J. W. Palmour, Appl. Phys. Lett. **105**, 182107 (2014).
[9]K. Kita, H. Hirai, H. Kajifusa, K. Kuroyama, and K. Ishinoda, Micro. Eng. **178**, 186 (2017).
[10]P. Fiorenza, F. Giannazzo, M. Vivona, A. La Magna, and F. Roccaforte, Appl. Phys. Lett. **103**, 153508 (2013).
[11]T. Hosoi, Y. Katsu, K. Moges, D. Nagai, M. Sometani, H. Tsuji, T. Shimura, and H. Watanabe, Appl. Phys. Express **11**, 091301 (2018).
[12]T. Umeda, G.-W. Kim, T. Okuda, M. Sometani, T. Kimoto, and S. Harada, Appl. Phys. Lett. **113**, 061605 (2018).
[13]J. L. Cantin, H. J. von Bardeleben, Y. Shishkin, Y. Ke, R. P. Devaty, and W. J. Choyke, Phys. Rev. Lett. **92**, 015502 (2004).
[14]J. L. Cantin, H. J. von Bardeleben, Y. Ke, R. P. Devaty, and W. J. Choyke, Appl. Phys. Lett. **88**, 092108 (2006).

[15]P. M. Lenahan and J. F. Conley, Jr., J. Vac. Sci. Technol. B **16**, 2134 (1998).
[16]C. J. Cochrane, P. M. Lenahan, and A. J. Lelis, J. Appl. Phys. **109**, 014506 (2011).
[17]T. Aichinger and P. M. Lenahan, Appl. Phys. Lett. **101**, 083504 (2012).
[18]G. Gruber, J. Cottom, R. Meszaros, M. Koch, G. Pobegen, T. Aichinger, D. Peters, and P. Hadley, J. Appl. Phys. **123**, 161514 (2018).
[19]T. Umeda, Y. Kagoyama, K. Tomita, Y. Abe, M. Sometani, M. Okamoto, S. Harada, and T. Hatakeyama, Appl. Phys. Lett. **115**, 151602 (2019) and references therein.
[20]T. Okuda, T. Kimoto, and J. Suda, Appl. Phys. Express **6**, 121301 (2013).
[21]K. Murakami, S. Tanai, T. Okuda, J. Suda, T. Kimoto, and T. Umeda, Mater. Sci. Forum **858**, 318 (2016).
[22]J. A. Weil, J. R. Bolton, and J. E. Wertz, *Electron Paramagnetic Resonance* (John Wiley & Sons, New York, 1994).
[23]J. Isoya, T. Umeda, N. Mizuochi, N. T. Son, E. Janzén, and T. Ohshima, Phys. Status Solidi B **245**, 1298 (2008).
[24]S. Greulich-Weber, Phys. Status Solidi B **210**, 415 (1998).
[25]C. J. Cochrane, P. M. Lenahan, and A. J. Lelis, Appl. Phys. Lett. **100**, 023509 (2012).
[26]T. Umeda, T. Kobayashi, M. Sometani, H. Yano, Y. Matsushita, and S. Harada, Appl. Phys. Lett. **116**, 071604 (2020).